Electrical properties of heteroepitaxial grown tin-doped indium oxide films

Naoaki Taga and Hidefumi Odaka
Research Center, Asahi Glass Co., Ltd., 1150 Hazawa-cho, Kanagawa-ku, Yokohama 221, Japan

Yuzo Shigesato[a] and Itaru Yasui
Institute of Industrial Science, University of Tokyo, 7-22-1 Roppongi, Minato-ku, Tokyo 106, Japan

Masayuki Kamei
Department of Materials Science and Technology, Science University of Tokyo, Noda, Chiba 278, Japan

T. E. Haynes
Solid State Division, Oak Ridge National Laboratory, Oak Ridge, Tennessee 37831

(Received 22 September 1995; accepted for publication 10 April 1996)

Oriented thin-film tin-doped indium oxide (ITO) was heteroepitaxially grown on optically polished (100) or (111) planes of single-crystalline yttria-stabilized zirconia (YSZ) substrates using e-beam evaporation or dc magnetron sputtering techniques. Pole figure x-ray diffraction analyses revealed that the heteroepitaxial relations were (001)ITO‖(001)YSZ, [100]ITO‖[100]YSZ, and (111)ITO‖(111)YSZ, [110]ITO‖[110]YSZ, respectively. X-ray rocking curve analyses and Rutherford backscattering spectrometry revealed that the e-beam evaporated heteroepitaxial ITO films had much higher crystallinity than the one deposited by dc magnetron sputtering. Both carrier density and Hall mobility of the e-beam evaporated heteroepitaxial films showed steady increases in a wide temperature range, which could be interpreted in terms of the increasing Sn-doping efficiency caused by the improvement of the crystallinity of In_2O_3 host lattice, and hence the decreasing Sn-based neutral scattering centers. © *1996 American Institute of Physics.* [S0021-8979(96)04614-2]

I. INTRODUCTION

Tin-doped indium oxide (ITO) is an *n*-type, highly degenerate, wide-gap semiconductor with an optical band gap more than 3.4 eV.[1] Due to its high transmissivity to visible light (more than 80%–90% at 550 nm) and its relatively low resistivity (lower than 2×10^{-4} Ω cm), ITO has been widely used as transparent conductive electrodes in various optoelectronic applications.[2–4] Free-carrier density of ITO can be increased through appropriate processing to a level of about 10^{21} cm^{-3}, where the free carriers are liberated from two different kinds of electron donor sites: substitutional tetravalent tin atoms $[Sn^{\cdot}]$ and divalent oxygen vacancies $[V_O^{\cdot\cdot}]$.[1] The electrically active tin atoms are supposed to be positioned substitutionally in the indium sites of the bixbyite In_2O_3 crystal structure. Considerable efforts have been focused on depositing thin-film ITO (thickness of 100–300 nm) with significantly reduced resistivity (lower than 1.5×10^{-4} Ω cm) in order to accommodate the increasing technological demand for larger area flat panel displays with higher image quality.[2,3] Several approaches to get the low resistivity films have been successfully made by using a number of techniques, including plasma-activated e-beam evaporation processes using either tungsten electron emitters[5,6] or an arc plasma generator,[7–9] rf magnetron sputtering,[10] and low voltage dc magnetron sputtering at decreased plasma impedance.[9,11] Scanning electron microscopy (SEM), transmission electron microscopy (TEM), and x-ray diffraction (XRD) analyses revealed that all of these films consisted of various sizes of In_2O_3 crystalline grains (10–500 nm) with various crystallographic preferred orientations depending on the deposition methods and their conditions.[9,12] Despite decades of research the reason for the low resistivity have not been thoroughly elucidated yet, probably because of the complex structure of unit cell of crystalline In_2O_3 (bixbyite I_{a3}) and the complicated nature of the conducting mechanisms in the polycrystalline structure.

Recently, well-oriented In_2O_3 films without large-angle grain boundaries have been fabricated using single-crystalline substrates of MgO or yttria-stabilized zirconia (YSZ).[13–15] Tarsa *et al.* reported on In_2O_3 films deposited by pulsed laser deposition that XRD rocking curve measurements revealed higher uniformity of surface-normal orientation of In_2O_3 on YSZ (rocking curve FWHM=0.29°) than the one on MgO (FWHM=1.5°), because of the smaller lattice mismatch of ~2% between In_2O_3 and YSZ ($a_{In_2O_3}=1.0118$ nm, $2a_{YSZ}=1.026$ nm) than In_2O_3 and MgO ($2a_{MgO}=0.842$ nm).[13] Investigations on the electrical conduction mechanisms of these heteroepitaxial films should be worth trying in order to find out the structural key factors that dominate the electrical properties of ITO.

In this study the carrier conduction mechanisms in heteroepitaxial ITO films deposited on YSZ single crystals by conventional e-beam evaporation or dc magnetron sputtering were investigated in a wide temperature range from 90 to 300 K, which was highly relevant to our interpretation on the carrier transport mechanism of the films. The difference in electrical properties between tin-doped and nondoped heteroepitaxial In_2O_3 films were also studied to investigate the intricate electrical behavior of tin doped in In_2O_3 films.

[a]Electronic mail: yuzo@iis.u-tokyo.ac.jp

 0021-8979/96/80(2)/978/7/$10.00

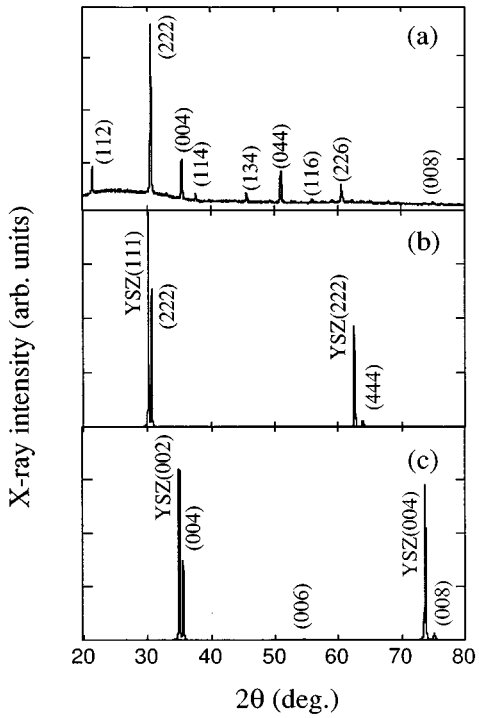

FIG. 1. X-ray diffraction (θ-2θ) patterns for ITO films grown on (a) a soda-lime glass substrate, (b) single crystalline YSZ(111), and (c) YSZ(100) substrates deposited by e-beam evaporation.

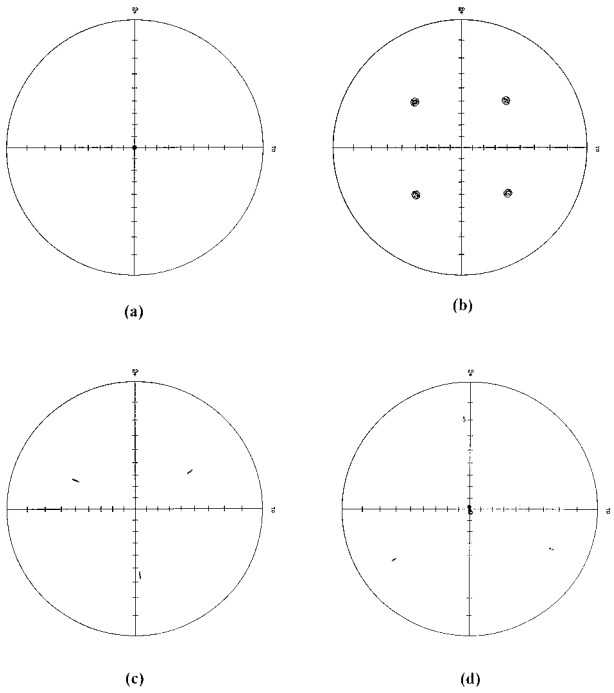

FIG. 2. Pole figures for (a) (004) diffraction, (b) (222) diffraction of the ITO grown on YSZ(001) and (c) (004) diffraction, (d) (222) diffraction of the ITO grown on YSZ(111) deposited by e-beam evaporation. Note that ITO/YSZ(001) showed excellent fourfold symmetry, whereas ITO/YSZ(111) showed threefold symmetry.

II. EXPERIMENT

A. Preparation of the films

Thin-film ITO with thickness of about 2000 Å was deposited on optically polished (001) or (111) planes of 1-mm-thick single-crystal yttria-stabilized zirconia [ITO/YSZ(001) or ITO/YSZ(111)] or on a soda-lime glass substrate (ITO/glass) at 300 °C using a conventional e-beam evaporation system. The conventional e-beam deposition system was evacuated to a background pressure smaller than 9×10^{-6} Torr and then filled with O_2 gas to 5×10^{-4} Torr. Sintered ITO pellets of 5 wt % SnO_2 content were used as an evaporating source, which could reduce spitting during evaporation rather than ITO powder. The O_2 partial pressure and the Sn concentration were the optimized values to obtain the films with the lowest resistivity for this system. For comparative purposes, pure In_2O_3 films were deposited on the YSZ [IO/YSZ(001) or IO/YSZ(111)] or on a soda-lime glass substrate (IO/glass) under the same deposition conditions. ITO films of approximately the same thickness were also deposited by conventional dc magnetron sputtering using a sintered oxide target with 10 wt % SnO_2 on the YSZ(100) or soda-lime glass substrates. The sputtering gas was a mixture of 99.2% Ar and 0.8% O_2 volume ratio and the total gas pressure during depositions was kept at 2.5×10^{-3} Torr.

B. Characterization of the films

Pole figure x-ray diffraction (PFXRD) analysis on the (222) or (004) diffraction of ITO by the Schultz reflection method was carried out with Cu $K\alpha$ radiation using a RINT 2500 with pole figure attachment (Rigaku Co. Ltd.). X-ray rocking curves were also measured using a Bede double-crystal diffractmeter (Rigaku Co. Ltd.) for precise evaluations on the uniformity of the crystalline grain orientation of the ITO/YSZ(001) deposited by the e-beam evaporation or the dc magnetron sputtering. The microstructure of the ITO/glass and ITO/YSZ(111) were observed by plan-view SEM images using a Hitachi S900 FE-SEM. The cross-sectional cleavage surface of ITO/YSZ(111) was also observed by the FE-SEM. The crystallographic disorder of the e-beam evaporated or sputtered heteroepitaxial ITO films was investigated by Rutherford backscattering spectrometry (RBS) using a High Voltage Engineering Model AN-2500 Positive Ion Accelerator. The ion channeling was carried out using 1.0 MeV He^+ ion beam at a scattering angle of 160°. Angular distribution of the ion channeling yield from In and Sn atoms was also measured around ⟨001⟩ growth axis.

The resistivity ρ, free-carrier density n, and Hall mobility μ of the films were measured by the four-point probe method and Hall-effect measurements in the van der Pauw geometry using a dc magnetic field of 6400 G. Ohmic contact between the probe and films was confirmed before each measurement. Film thicknesses were measured using a SLOAN Dektak 3030 apparatus. For selected samples, the temperature dependence of the ρ, n, and μ were measured over a temperature range from 90 to 300 K using liquid-nitrogen cooling.

III. RESULTS

Figures 1(a)–1(c) show conventional $\theta/2\theta$ x-ray diffraction (XRD) patterns for (a) ITO/glass, (b) ITO/YSZ(111),

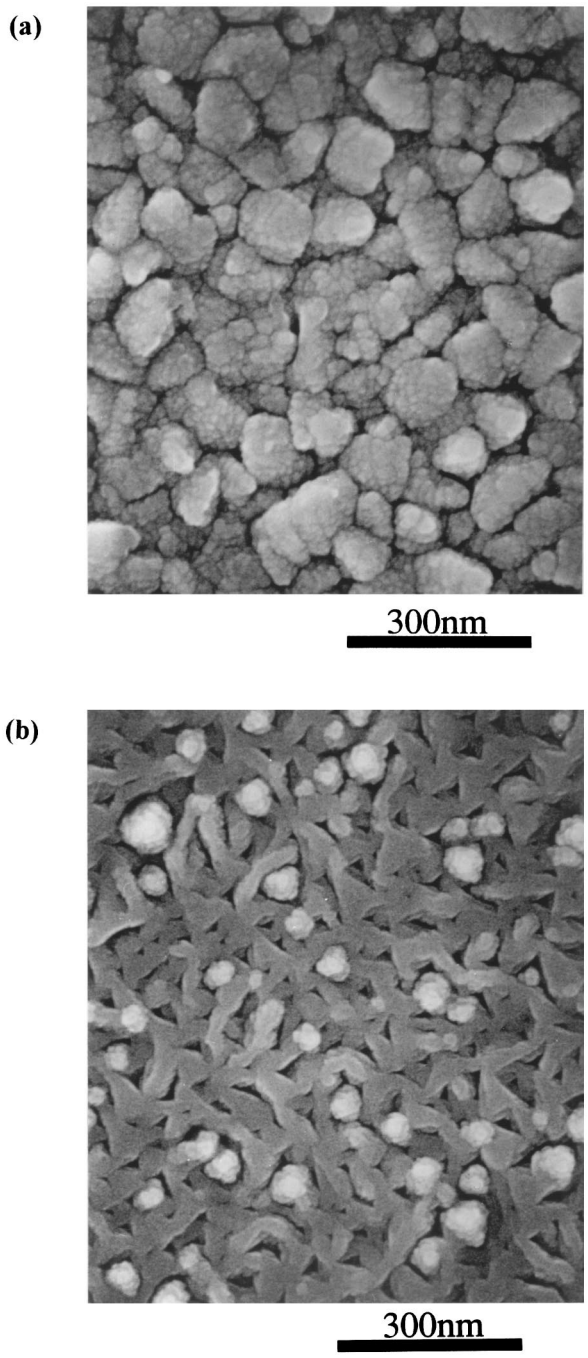

FIG. 3. Plan-view FE-SEM images of (a) ITO/glass and (b) ITO/YSZ(111) films deposited by e-beam evaporation. Note that in-plane-oriented, triangular-shaped crystallites are observed for (b) heteroepitaxial grown ITO/YSZ(111) film.

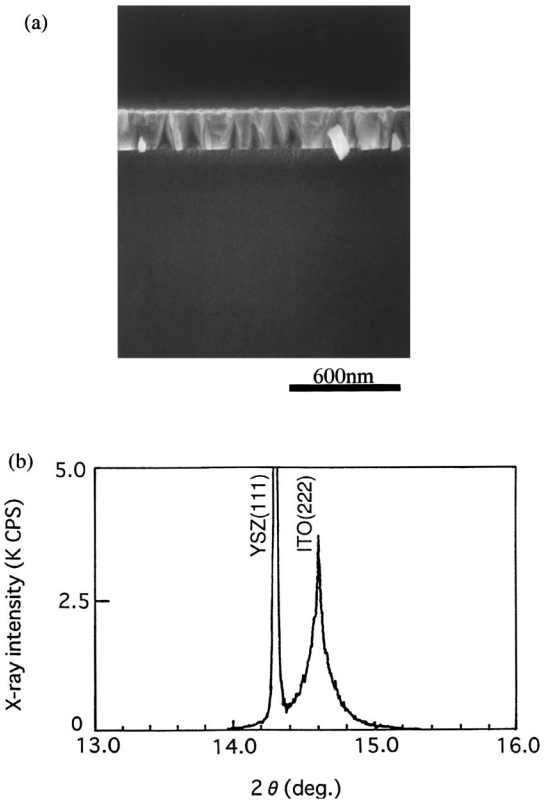

FIG. 4. (a) A cross-sectional FE-SEM image of ITO/YSZ(111) film deposited by e-beam evaporation. Note the columnar grains extending through the entire film thickness. (b) A rocking curve measured on the (222)In_2O_3 XRD peak (FWHM=0.049°).

and (c) ITO/YSZ(001) deposited by e-beam evaporation. All the XRD peaks of ITO/glass [Fig. 1(a)] could be assigned to the cubic bixbyite structure of In_2O_3 without any SnO_2, Sn-metal, or In-metal peaks. The integrated intensity ratio of (004) peak to (222) peak for ITO/glass was 0.29, which was close to the value of 0.33 for the random orientation from JCPDS (Joint Committee on Powder Diffraction Standards) indicating that the ITO/glass consisted of the crystalline grains with almost random orientation. Whereas the XRD patterns of ITO/YSZ(111) [Fig. 1(b)] or ITO/YSZ(001) [Fig. 1(c)] showed only intense peaks of ITO(hhh) or ITO($00k$) diffraction (h,k=integer), respectively, indicating that the ITO films deposited on YSZ(111) or (001) had preferential ⟨111⟩ or ⟨001⟩ orientations normal to the surface. Figures 2(a)–2(d) show pole figure x-ray diffraction (PFXRD) patterns for the films grown on the YSZ single-crystal substrates. From the PFXRD pattern of ITO/YSZ(001), a very sharp and intense (004) diffraction was observed at the origin of the stereographic projection [Fig. 2(a)], and (222) diffractions were at an angle of 55° from the origin making a clear fourfold rotation symmetry around the ⟨004⟩ axis [Fig. 2(b)]. In the case of a cubic structure, the angle between the ⟨222⟩ axis and the ⟨004⟩ axis was calculated to be 54.75°, which was in good agreement with the value observed in Fig. 2(b). On the other hand, from the pattern of ITO/YSZ(111), very sharp (004) diffraction points were observed at an angle of 55° from the origin of the stereographic projection showing a clear threefold rotation symmetry [Fig. 2(c)]. Very sharp (222) diffractions were also observed at the origin and at three other equivalent points at an angle of 71° from the origin, showing a clear threefold rotation symmetry [Fig. 2(d)]. This angle of 71° was also in good agreement with the calculated angle of 70.53° between each ⟨222⟩ axis in a cubic structure. These PFXRD patterns indicate an excellent in-plane crystalline orientation without large-angle grain boundaries. The orientation relations between ITO films and YSZ substrates obtained from the PFXRD patterns were

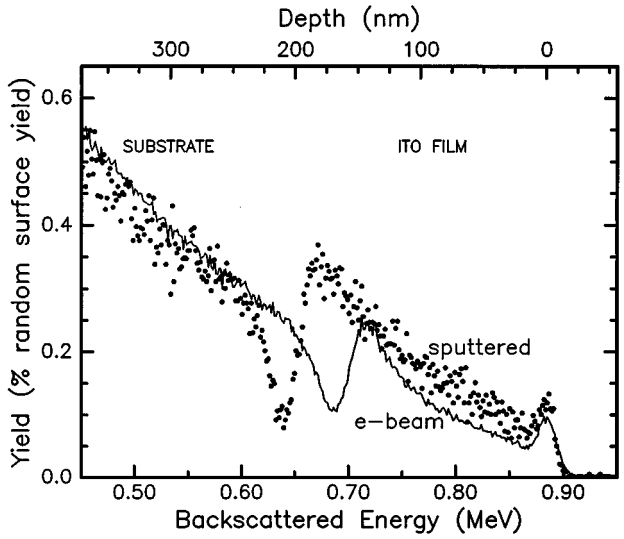

FIG. 5. Ion channeling spectra taken along the ⟨100⟩ growth axis from e-beam evaporated (line) and magnetron sputtered (points) ITO films deposited on YSZ(100) substrates at T_s=300 °C. Backscattered 1.0 meV He^+ ions were detected at a scattering angle of 160°.

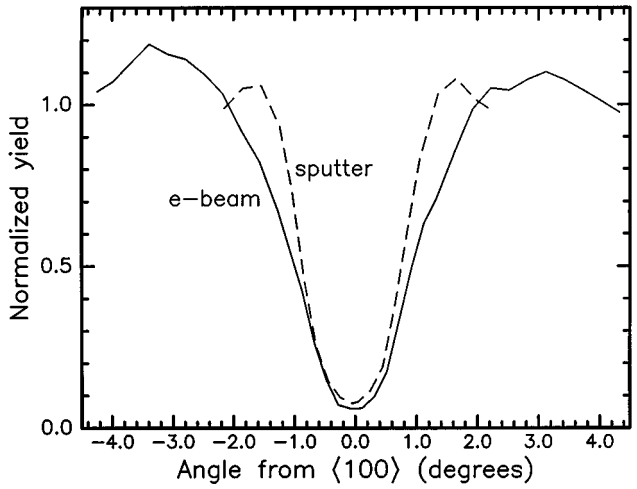

FIG. 6. Angular distribution of the ion channeling yield from In+Sn atoms measured around the ⟨100⟩ growth axis for 1.0 MeV He^+ ions incident on the e-beam (solid) and sputtered (dashed) ITO films.

(001)ITO‖(001)YSZ, [100]ITO‖[100]YSZ for the ITO/YSZ(001) and (111)ITO‖(111)YSZ, [110]ITO‖[110]YSZ for the ITO/YSZ(111), respectively.

Figure 3 shows the SEM surface images of the ITO/glass [Fig. 3(a)] and ITO/YSZ(111) [Fig. 3(b)] deposited by e-beam evaporation. The ITO/glass consisted of nonequilibrium shaped grains with size of 50–150 nm. Whereas the ITO/YSZ(111) consisted of in-plane oriented, triangular-shaped grains indicating an excellent in-plane crystalline orientation of this film. The SEM image of cleavage surface of ITO/YSZ(111) is also shown in Fig. 4(a). Note that a clear columnar growth of each crystalline grain can be observed throughout the film thickness. Figure 4(b) shows an x-ray rocking curve measured on the (222) ITO and the (111) YSZ peak for the ITO/YSZ(111). This result (rocking curve FWHM=0.049°) indicates that the heteroepitaxial ITO/YSZ(111) deposited by e-beam evaporation has grown with much higher uniformity of crystalline orientation with the comparison of the sputter-deposited film (rocking curve FWHM=0.53°).

An ion channeling spectrum from the heteroepitaxial ITO film deposited on a YSZ(100) substrate [ITO(100)/YSZ(100)] by e-beam evaporation is compared to that deposited by dc magnetron sputtering at the same substrate temperature of 300 °C in Fig. 5. The minimum yield from the e-beam evaporated film is 4.5%, which is better than that from the sputter-deposited film (8.0%). The difference in minimum yield is direct evidence that the e-beam evaporated films have fewer crystal defects. The angular dependence of the scattering yields from these same two samples is compared in Fig. 6. The width of the angular distribution is somewhat broader for the e-beam deposited film. Since extended defects, strain, or crystallite misorientation increase the angular divergence of the analysis beam within the crystal, a larger minimum yield arising from these types of defects should be associated with a broader angular distribution. However, that is not the case here. Instead, when the large minimum yield is coupled with a narrower angular distribution, as for the sputter-deposited films in Fig. 6, this indicates that a fraction of the atoms are displaced individually just slightly (<0.05 nm)[16] from their lattice sites. So we can conclude that the defects that cause the relatively larger minimum yield in the sputter deposited film are not extended defects but point defects that displace individual In and/or Sn atoms from their lattice sites by <0.05 nm, as measured perpendicular to the ⟨100⟩ direction.

The room-temperature resistivity ρ, carrier density n, and Hall mobility μ, of the e-beam deposited ITO(001)/YSZ(001) and ITO(111)/YSZ(111) are shown in Tables I and II, respectively, in comparison with those of ITO/glass deposited simultaneously in the same batch. Note that the ρ of both heteroepitaxial ITO films were significantly smaller than ITO/glass. ρ of ITO(001)/YSZ(001) decreased from 2.7×10^{-4} to 1.2×10^{-4} Ω cm due to the increase both in n from 9.5×10^{20} to 1.4×10^{21} cm^{-3} and in μ from 23 to 38 cm^2/V s, respectively. ρ of ITO(111)/YSZ(111) also de-

TABLE I. Electrical properties of the ⟨100⟩-oriented heteroepitaxial ITO film on a YSZ(001) single-crystal and polycrystalline ITO film on a glass substrate deposited by e-beam evaporation simultaneously in the same batch.

	Resistivity ($\times10^{-4}$ Ω cm)	Hall mobility (cm^2/V s)	Carrier density ($\times10^{20}$ cm^{-3})	Neutral scattering center density ($\times10^{20}$ cm^{-3})
Glass substrate	2.7	23	9.5	1.4–2.0
YSZ substrate (100)	1.2	38	14.0	0.2–0.9

TABLE II. Electrical properties of the ⟨111⟩-oriented heteroepitaxial ITO film on a YSZ(111) single-crystal and polycrystalline ITO film on a glass substrate deposited by e-beam evaporation simultaneously in the same batch.

	Resistivity ($\times 10^{-4}$ Ω cm)	Hall mobility (cm^2/V s)	Carrier density ($\times 10^{21}$ cm^{-3})	Neutral scattering center density ($\times 10^{20}$ cm^{-3})
Glass substrate	2.3	27	1.0	1.0–1.6
YSZ substrate (111)	1.3	41	1.3	0.2–0.8

creased from 2.3×10^{-4} to 1.3×10^{-4} Ω cm due to both increases in n and μ, from 1.0×10^{21} to 1.3×10^{21} cm^{-3} and from 27 to 41 cm^2/V s, respectively. The electrical properties of heteroepitaxial nondoped In_2O_3 films [IO(001)/YSZ(001) or IO(111)/YSZ(111)] and In_2O_3 on the soda-lime glass substrate (IO/glass) deposited simultaneously in the same batch were also measured in order to investigate the Sn-doping effect (Table III). The IO films showed larger ρ than the ITO films by one order of magnitude due to much smaller n. Also for the nondoped films, ρ of the both heteroepitaxial IO films (1.5×10^{-3} or 1.6×10^{-3} Ω cm) was smaller than that of IO/glass (2.0×10^{-3} Ω cm). In this case, the μ of the heteroepitaxial films (about 70 cm V/s) was larger than IO/glass (55 cm V/s), whereas n was almost the same for the all three IO films. Note that differences in the electrical properties between IO(001)/YSZ(001) and IO(111)/YSZ(111) were not observed indicating that the electrical properties of cubic In_2O_3 are isotropic, which is consistent with the results on well-oriented ITO films deposited on ZnO film-coated glass substrates.[17]

IV. DISCUSSION

The electrical properties of the e-beam deposited heteroepitaxial ITO/YSZ films were considerably improved as compared with to those of simultaneously deposited ITO/glass films (Tables I, II), reasons for which must be worth discussing in order to evaluate the key structural factors for the lower resistivity. Low-temperature Hall-effect measurements were carried out to investigate the carrier transport mechanisms in both films. The ρ, n, and μ of the heteroepitaxial ITO(100)/YSZ(100) (closed squares) and the ITO/glass (closed circles) films are shown in Fig. 7 as a function of measurement temperature in a range from 300 to 90 K. As is typical for a highly degenerate semiconductor,[18] both films showed a slight decrease in mobility in the temperature range from RT to 200 K and showed almost a constant value below 200 K. Based on these data, it is reasonable to assume that electron scattering at dislocations,[19] acoustic phonons or polar optical phonons,[20] which have large temperature dependence, are unimportant for this material. Carrier scattering at grain boundaries is sometimes postulated in metal or semiconductor polycrystalline films with small crystallite size.[21] The grain boundary scattering, however, also seems to be less important in this material, because the mean-free path of electrons at the Fermi surface calculated using a highly degenerate electron gas model was always much smaller than the grain size by more than an order of magnitude.[18,22,23] As such, it appears that the carrier mobilities in ITO films are mainly dominated by neutral scattering centers which are independent of temperature[23] and by ionized scattering centers[25] which possibly explains the slight observed temperature dependence above 200 K using the Fermi-Dirac distribution function.[26] The mobilities dominated only by the neutral scattering centers μ_N, or the ionized scattering centers μ_I, in degenerate semiconductors have been previously described[24,25,29] as follows:

$$\mu_N=(m^*e^3)/(20\epsilon_0\epsilon_r\hbar^3 n_N) \tag{1}$$

$$\mu_I=[24\pi^3(\epsilon_0\epsilon_r)^2\hbar^3 n]/[e^3 m^{*2} g(x) Z^2 n_I], \tag{2}$$

where the screening function $g(x)$ is given by

$$g(x)=\ln(1+4/x)-(1+x/4)^{-1}, \tag{3}$$

and where

$$x=(4e^2m^*)/[4\pi\epsilon_0\epsilon_r\hbar^2(3\pi^5)^{1/3}n^{1/3}]. \tag{4}$$

Here ϵ_r is the low-frequency relative permittivity for which a value for ITO of 9 is commonly selected,[1] n_N the density of the neutral scattering centers, Z and n_I are the charge and the density of the ionized scattering centers, and a value of $0.3m_e$ is used for m^*.[1,27] The values of n/n_IZ^2 in Eq. (2) for $[V_O^{\cdot\cdot}]$ and $[Sn^{\cdot}]$ are 0.5 and 1, respectively. In order to obtain the lower resistivity films, n_N, which does not contribute to the increase in n but increases the carrier scattering, should be minimized. The value n_N could be estimated for each film through the formula $1/\mu=1/\mu_N+1/\mu_I$

TABLE III. Electrical properties of the ⟨100⟩- or ⟨111⟩-oriented heteroepitaxial In_2O_3 films on YSZ (001) or (111) single-crystals and polycrystalline In_2O_3 film on a glass substrate deposited by e-beam evaporation simultaneously in the same batch.

	Resistivity ($\times 10^{-3}$ Ω cm)	Hall mobility (cm^2/V s)	Carrier density ($\times 10^{19}$ cm^{-3})	Neutral scattering center density ($\times 10^{19}$ cm^{-3})
Glass substrate	2.0	55	5.8	3.7
YSZ substrate (100)	1.5	73	5.9	1.2
YSZ substrate (111)	1.6	70	5.6	1.6

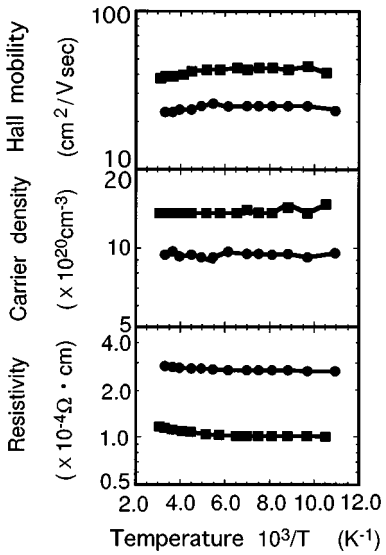

FIG. 7. Effect of measurement temperature on resistivity, carrier density, and Hall mobility of the ITO/glass (closed circles) and ITO/YSZ(100) (closed squares) films deposited by e-beam evaporation at T_s=300 °C.

with the assumption that all the donors were liberated from $[V_O^{\cdot\cdot}]$ or $[Sn^{\cdot}]$ which were the only source for the ionized scattering centers (Tables I, II, and III).

The change in the neutral scattering center n_N seems to give good explanations for the differences in the carrier mobility between ITO/YSZ and ITO/glass (Tables I, II). The n_N values for both ITO/YSZ(100) and ITO/YSZ(111) were smaller than the one of ITO/glass by about 1×10^{20} cm^{-3}, where the carrier density n were larger for the heteroepitaxial films by $3–4\times10^{20}$ cm^{-3}. The origins for the neutral scattering centers have been presumed to be two different kinds of crystallographic faults, i.e., (1) point defect aggregates which were observed by TEM as locally strained small areas and supposed to be low-grade oxide of In_2O_3, $[In_2O_{3-x}]$,[28] or (2) an interstitial or associated Sn-oxide defect complexes such as $[Sn_2^{\cdot}O_i'']$, $[Sn_2O_4]^x$ or $[[Sn_2^{\cdot}O_i''][Sn_2O_4]^x]$ which were electrically inactive and did not contribute to the increase in n.[22,29] The difference in the n_N values between nondoped IO/YSZ(001) or (111) and IO/glass was only $2–2.5\times10^{19}$ cm^{-3} (Table III), indicating the decrease in n_N by the heteroepitaxial growth that could be assigned to decreasing native defect aggregates (1). On the other hand, the decrease in n_N by the heteroepitaxial growth in Sn-doped films was about quintuple as larger as the one for nondoped IO films. Therefore the larger n and smaller n_N of the ITO/YSZ as compared to ITO/glass should be mainly attributable to the increase in the electrically active substitutional tetravalent Sn atoms ($[Sn^{\cdot}]$) at In sites.

It has been reported[30,31] that Sn in amorphous ITO (*a*-ITO) films is not electrically active and does not contribute carriers to the amorphous material. When these *a*-ITO films are crystallized by post annealing in air, the Sn becomes electrically active. Therefore the higher Sn-doping efficiency for ITO/YSZ than ITO/glass, by which the higher μ and n were achieved, was thought to be caused by the steady improvement of the crystallinity with the heteroepitaxial growth. Muranaka *et al.* reported on TEM analysis of ITO films with various thicknesses deposited by e-beam evaporation on a glass substrate, in which very thin films of 5–20 nm thickness deposited at T_s=150–200 °C consisted of a large amount of amorphous layer though the T_s was higher than crystallization temperature of 150 °C.[32] Such an amorphous structure close to the substrate surface was considered to be caused by the random atomic configuration of the glass substrate surface because heteroepitaxial growth of ITO films on YSZ was confirmed at T_s=200 °C.[14,15] Recently, ITO films deposited by sputtering or ion plating at T_s=150–200 °C on SiO_2-coated glass substrates were reported to consist of two differently strained layers, which also originated in the amorphous substrate surface structure.[33] Based on these reports the lower crystallinity of the ITO/glass than the ITO/YSZ are considered to be results of the interaction between ITO films and the atomically random surface of the glass substrate during early stages of the film growth.

Electrical properties of ITO/YSZ(100) and ITO/glass deposited by dc magnetron sputtering[14] are also shown in Table IV with the ones by e-beam evaporation for comparative purposes. Note that both of μ and n values, and hence n_N, were almost the same for the sputtered ITO/YSZ and ITO/glass. The different relaxation of the uniform strain, i.e., the change in the lattice parameter, with increasing film thickness was reported between ITO films deposited by e-beam evaporation and dc sputtering on glass substrates.[34] According to the report, the uniform strain of the e-beam evaporated films, which was larger than 1.0% for films thinner than 100 nm, converged very rapidly with the film growth and became the same value as that of ITO powder, 0.2%, at a thickness of 250 nm. Whereas the convergence was slower for the sputter deposited films and uniform strain still remained 0.6% even at a thickness of 760 nm. In the sputter deposition processes two kinds of high-energy particles have been reported to bombard the growing film surface, i.e., (1) high-energy neutrals (Ar°) produced by neutralization of positive ions (Ar^+)

TABLE IV. Electrical properties of the ⟨100⟩-oriented heteroepitaxial ITO film on YSZ(001) single-crystals and polycrystalline ITO film on a glass substrate deposited by magnetron sputtering (see Ref. 14).

	Resistivity ($\times10^{-4}$ Ω cm)	Hall mobility (cm^2/V s)	Carrier density ($\times10^{20}$ cm^{-3})	Neutral scattering center density ($\times10^{20}$ cm^{-3})
Glass substrate	2.0	41	7.5	0.3–0.9
YSZ substrate (100)	2.2	39	7.3	0.4–1.0

at the surface of the target[35] and (2) energetic negative ions (O^-) accelerated in the cathode sheath to the substrate surface.[36] The improvement of the crystallinity for the sputter deposited ITO/YSZ was suppressed with the comparison of the e-beam evaporated ITO/YSZ (Fig. 5) maybe because of such energetic particle bombardments during film growth, which should be the reason for the similar electrical properties between sputter deposited ITO/YSZ and ITO/glass.

After all, the chemical states of Sn in ITO films, and hence the doping efficiency of Sn, should be an important key factor to increase both n and μ. The improvement in crystallinity of the In_2O_3 host lattice seems to have certain effects to increase the doping efficiency, which should be achieved by suppressing the influences of the random atomic configuration of the substrate surface and suppressing the damage caused by the energetic particle bombardment during the film growth.

V. CONCLUSION

Heteroepitaxial growth of the ITO films was achieved on both YSZ(111) and YSZ(100) substrates using conventional e-beam evaporation. Pole figure XRD analyses revealed that the heteroepitaxial relations were (001)ITO‖(001)YSZ, [100]ITO‖[100]YSZ, and (111)ITO‖(111)YSZ, [110]ITO‖[110]YSZ, respectively. Steady decrease in the resistivity was observed for the heteroepitaxial films in a wider temperature range, which originated in an increasing carrier density (n) and a decreasing neutral scattering center density (n_N). The comparison with the results on nondoped In_2O_3/YSZ revealed that such neutral scattering centers were considered to originate mainly in electrically inactive Sn which did not contribute to the carrier density. The improvement in crystallinity of the In_2O_3 host lattice seems to have certain effects to decrease n_N and to increase the Sn-doping efficiency, which could decrease the dopant trapped at crystalline defects and hence automatically increase electrically active species inside each grain. The suppression of the influence of the random atomic configurations of substrate surface on the early stages of the film growth and the suppression of damage caused by the energetic particle bombardment during the film growth were proved to be important key factors to deposit ITO films with extremely low resistivity.

ACKNOWLEDGMENTS

Part of this research was performed at Oak Ridge National Laboratory and sponsored by the U.S. Department of Energy under Contract No. DE-AC05-84OR21400 with Martin Lockheed Energy Systems, Inc.

[1] I. Hamberg and C. G. Granqvist, J. Appl. Phys. **60**, R123 (1986).
[2] T. Kamimori, J. Nagai, and M. Mizuhashi, Sol. Energy Mater. **16**, 27 (1987).
[3] H. Koh, K. Sawada, M. Ohgawara, T. Kuwata, M. Akatsuka, and M. Matsuhiro, SID Tech. Dig. **19**, 53 (1988).
[4] H. Kobayashi, T. Ishida, Y. Nakato, and H. Tsubomura, J. Appl. Phys. **69**, 1736 (1991).
[5] P. Nath, R. F. Bunshah, B. M. Masel, and O. M. Stuffsud, Thin Solid Films **72**, 463 (1980).
[6] S. Takaki, K. Matsumoto, and K. Suzuki, Appl. Surf. Sci. **33/34**, 919 (1988).
[7] T. Oyama, N. Hashimoto, J. Shimizu, Y. Akao, H. Kojima, K. Aikawa, and K. Suzuki, J. Vac. Sci. Technol. A **10**, 1682 (1992).
[8] K. Suzuki, N. Hashimoto, T. Oyama, J. Shimizu, Y. Akao, and H. Kojima, Thin Solid Films **226**, 104 (1993).
[9] Y. Shigesato, S. Takaki, and T. Haranoh, J. Appl. Phys. **71**, 3356 (1992).
[10] S. Ray, R. Banerjee, N. Basu, A. K. Batabyal, and A. K. Barna, J. Appl. Phys. **54**, 3497 (1983).
[11] S. Ishibasi, Y. Higuchi, Y. Ota, and K. Nakamura, J. Vac. Sci. Technol. A **8**, 1403 (1990).
[12] Y. Shigesato and D. C. Paine, Thin Solid Films **238**, 44 (1994).
[13] E. J. Tarsa, J. H. English, and J. S. Speck, Appl. Phys. Lett. **62**, 2332 (1993).
[14] M. Kamei, T. Yagami, S. Takai, and Y. Shigesato, Appl. Phys. Lett. **64**, 2712 (1994).
[15] M. Kamei, Y. Shigesato, S. Takaki, Y. Hayashi, M. Sasaki, and T. E. Haynes, Appl. Phys. Lett. **65**, 546 (1994).
[16] Due to the phenomenon of flux peaking in ion channeling, larger atomic displacements would induce a peak at the center of the angular scan, which is not observed in Fig. 6. See, for example, L. C. Feldman, J. W. Mayer, and S. T. Picraux, *Materials Analysis by Ion Channeling* (Academic, New York, 1982), pp. 76–79.
[17] C. H. Yi, I. Yasui, and Y. Shigesato, Jpn. J. Appl. Phys. **34**, 1638 (1995).
[18] T. M. Ratcheva, M. D. Nanova, L. V. Vassilev, and M. G. Mikhailov, Thin Solid Films **139**, 189 (1986).
[19] D. L. Dexter and F. Seitz, Phys. Rev. **86**, 964 (1952).
[20] C. G. Fonstad and R. H. Rediker, J. Appl. Phys. **42**, 2911 (1971).
[21] M. Higuchi, M. Sawada, and Y. Kuronuma, J. Electrochem. Soc. **140**, 1773 (1993).
[22] Y. Shigesato and David C. Paine, Appl. Phys. Lett. **62**, 1268 (1993).
[23] Y. Shigesato, David C. Paine, and T. E. Haynes, J. Appl. Phys. **73**, 3805 (1993).
[24] C. Erginsoy, Phys. Rev. **79**, 1013 (1950).
[25] R. B. Dingle, Philos. Mag. **46**, 831 (1955).
[26] A. Fujisawa, T. Nishino, and Y. Hamakawa, Jpn. J. Appl. Phys. **27**, 552 (1988).
[27] R. Clanget, Appl. Phys. **2**, 247 (1973).
[28] Y. Shigesato, David C. Paine, and T. E. Haynes, Jpn. J. Appl. Phys. **32**, L1352 (1993).
[29] G. Frank and H. Köstlin, Appl. Phys. A **27**, 197 (1982).
[30] Y. Shigesato, Y. Hayashi, and T. Haranoh, Appl. Phys. Lett. **61**, 73 (1992).
[31] J. R. Bellingham, W. A. Phillips, and C. J. Adkins, J. Phys. **2**, 6207 (1990).
[32] S. Muranaka, Y. Bando, and T. Takeda, Thin Solid Films **151**, 335 (1987).
[33] C. H. Yi, Y. Shigesato, I. Yasui, and S. Takaki, Jpn. J. Appl. Phys. **34**, L244 (1995).
[34] Y. Shigesato, S. Takaki, and T. Haranoh, Appl. Surf. Sci. **48/49**, 269 (1991).
[35] I. Brodie, L. T. Lamont, Jr., and R. J. Jepsen, Phys. Rev. Lett. **21**, 1224 (1968).
[36] K. Tominaga, M. Chong, and Y. Shintani, J. Vac. Sci. Technol. A **12**, 1435 (1994).